

On the efficiency of pairwise Hamiltonian control to desynchronize the higher-order Kuramoto model

Martin Moriamé,¹ Riccardo Muolo,^{2,3} Timoteo Carletti,¹ and Maxime Lucas^{1,4}

¹⁾*Department of Mathematics and Namur Institute for Complex Systems (naXys), University of Namur, 5000 Namur, Belgium*

²⁾*RIKEN Center for Interdisciplinary Theoretical and Mathematical Sciences (iTHEMS), Saitama 351-0198, Japan*

³⁾*Department of Systems and Control Engineering, Institute of Science Tokyo (former Tokyo Tech), Tokyo 152-8552, Japan*

⁴⁾*Earth and Life Institute, Mycology, Catholic University of Louvain, B-1348 Louvain-la-Neuve, Belgium*

(*Electronic mail: martin.moriamé@unamur.be)

(Dated: 18 February 2026)

Synchronization of coupled oscillators is observed in many natural and engineered systems and emerges due to the interactions within the system. It can be both beneficial, e.g., in power grids, and harmful, e.g., in epileptic seizures. In the latter case, efficient control methods to desynchronize the systems are crucial. Recent studies have shown that interactions are not always pairwise, but higher-order, i.e., many-body, and this greatly affects the dynamics. For instance, higher-order interactions increase the linear stability of synchronized states but simultaneously shrink their attraction basin, with potentially opposite effects on control methods. Here, we use a minimally invasive pairwise control based on Hamiltonian control theory, and investigate its efficiency on phase oscillators with higher-order interactions. We show that, if the initial phases are close to the synchronized state, higher-order interactions make desynchronization more difficult to achieve. Otherwise, a non-monotonic effect appears: intermediate strengths of higher-order interactions impede desynchronization while larger ones facilitate it. In all cases, the control can desynchronize the system with a sufficient number of controlled nodes and intensity.

Many natural and engineered systems are composed of ensembles of interacting oscillators. When the interactions are strong enough, the oscillators may synchronize, meaning that they evolve with the same rhythm. While synchronization can be useful in many applications, there are important cases, e.g., in brain dynamics, in which it can be harmful and needs to be controlled and reduced. Pairwise interactions have been largely used to model coupled oscillators. However, increasing evidence shows that interactions are often higher-order, i.e., involving more than two oscillators at a time. Such interactions dramatically shape the dynamics, providing a plethora of synchronization patterns. In this work, we examine how such higher-order interactions influence the effectiveness of a simple control strategy designed to desynchronize a population of coupled oscillators. By studying different initial conditions and interaction strengths, we provide a clearer picture of when higher-order interactions make desynchronization harder or easier to achieve.

I. INTRODUCTION

Synchronization is one of the most astonishing examples of self-organization in complex systems. Since its description by Huygens in the 1600s, the synchronization of coupled oscillators has been observed in many natural and engineered systems, and finds applications from health and neuroscience to mechanics and power grids^{1–5}. Since Kuramoto proposed his canonical model with all-to-all coupling^{6,7}, the

effect of complex network structures has been investigated in many extensions^{8,9}. In general, synchronization can be beneficial to the system, for example, in cardiac dynamics¹⁰ and power grids¹¹; but it can also be harmful in other contexts, such as mechanics¹², aviation^{13–15}, or neuroscience^{16–19}. For example, neurons are known to synchronize at the onset of epileptic seizures^{20,21}. In such cases, one wants to be able to desynchronize the system.

Control theory offers several approaches to achieve synchronization including optimal control^{22–24}, pinning control^{25–31}, or adaptive control^{14,28,30,32}, to name a few. Let us however observe that the literature dealing with desynchronization is more rare^{33–37}.

One relevant research line aimed at desynchronizing coupled oscillators originated with Ref. [33]. It relies on the idea of embedding the Kuramoto model into a Hamiltonian system³⁸, to then leverage Hamiltonian control theory^{39,40} to build a pinning control strategy aimed at desynchronizing the system. In Ref. [35], Asllani *et al.* went a step further by introducing a modified control that results to be minimally invasive—the control magnitude is proportional to the level of synchronization and thus acts only when necessary—and requires less knowledge of the system parameters, making it easier to implement in practice.

Recent evidence suggests that, in many systems, interactions tend to be higher-order, i.e., between more than two nodes, rather than just pairwise as in the traditional framework described above^{41–48}. Consequently, the interactions are more accurately described by generalization of pairwise networks, such as hypergraphs and simplicial complexes. Importantly, higher-order interactions have been shown to dramatically af-

fect dynamics, e.g., with chaotic oscillators^{49–51}, swarming and active matter^{52–54}, chimera states^{55,56}, stochastic resonance⁵⁷, pattern formation^{58,59}, opinion dynamics^{60–65}, and random walks^{66–68}, to name a few.

In systems of coupled phase oscillators, i.e., higher-order Kuramoto models⁶⁹, higher-order interactions have been shown to naturally arise from phase reduction^{70–74}, and to induce multi-stability, chaos, and explosive transitions, among others^{75–90}. Recently, an interesting effect was described, that is of particular interest for this study: higher-order interactions can make the attraction landscape of synchronized states such as twisted states, “deeper but smaller”, that is, increasing higher-order coupling strength increases linear stability but shrinks attraction basins⁹¹.

Early efforts have started to adapt control methods to modulate the synchronization of oscillators with higher-order interactions^{37,92–100}. In particular, building on Refs. [33 and 35], a higher-order Hamiltonian control scheme was defined by embedding a higher-order Kuramoto model into a Hamiltonian system¹⁰⁰. This higher-order version of the control was shown to be able to desynchronize the higher-order Kuramoto model better than the pairwise control, when higher-order interactions are not too weak. In cases where pairwise interactions are prominent, the higher-order control also worked, but the pairwise control was sufficient. However, the higher-order extension makes the control terms more expensive to compute and to implement; to obtain a simplified minimally invasive version of the latter seems to be a hard task to achieve. Thus, being able to control a higher-order system with the pairwise minimally invasive method developed in [35] remains of great interest.

In the context of the “deeper but smaller” effect induced by higher-order interactions, a natural question arises: how is the desynchronization control affected by higher-order interactions? Indeed, the increased linear stability would tend to make desynchronization harder, but the reduced size of the attraction basin would have the opposite effect. The result of these two competing effects on the efficiency of the control remains unclear.

In the present work, we aim to answer this question. To do so, we assess the ability of a minimally invasive pairwise control³⁵ to desynchronize systems composed of oscillators coupled with higher-order networks. We test the effect of both the intensity of higher-order interactions and the initial distance to the center of the attraction basin. We first found that, for initial conditions starting close to the fully synchronized state, the stronger the higher-order interactions, the less efficient the control. On the other hand, for less synchronized initial conditions, we found a non-monotonic behavior. While intermediate magnitudes of higher-order interactions hinder the control efficiency, higher ones improve it. These results are consistent with the behavior of uncontrolled systems^{91,101–104}.

The manuscript is organized as follows. In Section II we present the higher-order Kuramoto model and the pairwise minimally invasive control method we adapted from [35]. In Sections III and IV we develop and show the results of our numerical experiments where initial conditions are, resp., synchronized or randomly deviated from synchronization. We

then wrap up and conclude in Section V.

II. THE MODEL

Let us consider the following system of N coupled phase oscillators^{77,91}

$$\begin{aligned} \dot{\theta}_i = \omega_i + \frac{K_1}{\langle k^{(1)} \rangle} \sum_{j=1}^N A_{ij}^{(1)} \sin(\theta_j - \theta_i) \\ + \frac{K_2}{\langle k^{(2)} \rangle} \sum_{j,k=1}^N A_{ijk}^{(2)} \sin(\theta_j + \theta_k - 2\theta_i) + \mu \delta_i p_i, \end{aligned} \quad (1)$$

where $\theta_i \in [0, 2\pi]$ is the phase of the i -th oscillator, and ω_i its natural frequency, drawn from a normal distribution $\omega \sim \mathcal{N}(0, \sigma^2)$ with variance σ^2 . Interactions are determined, at orders 1 and 2, by the respective adjacency tensors $\mathbf{A}^{(1)}$ and $\mathbf{A}^{(2)}$, and coupling strengths $K_1 \geq 0$ and $K_2 \geq 0$. The full coupling strengths are normalized by the associated mean degrees $\langle k^{(1)} \rangle$ and $\langle k^{(2)} \rangle$ so that K_1 and K_2 can be fairly compared.

Finally, node i is controlled by p_i with strength $\mu \geq 0$ if $\delta_i = 1$ ($= 0$ otherwise, namely the node is not directly controlled). The control term will be defined hereafter in Eq. (3). Note that here, for the sake of simplicity, we restrain higher-order interactions to three-body ones. Equation (1) without control (i.e., $\mu = 0$) is an extension¹⁰⁵ of the Kuramoto model^{77,89,91}. Such models are known to synchronize under certain conditions, and the level of synchronization is typically characterized by the Kuramoto order parameter R , defined as

$$Re^{i\Psi} = \frac{1}{N} \sum_{j=1}^N e^{i\theta_j}, \quad (2)$$

where $i = \sqrt{-1}$ is the imaginary unit. The value of R lies in $[0, 1]$, with $R = 0$ corresponding to a uniform distribution of the phases in $[0, 2\pi]$ and $R = 1$ to perfect synchronization in which all phases θ_i are equal. Note that the latter is an equilibrium only for systems with identical frequencies $\omega_i = \omega$. For distributed frequencies, a state in which R is close to 1 is stable instead; we refer to it as the fully synchronized state. Note that the Kuramoto model describes the dynamics of phase oscillators, which may be restrictive for potential applications, given that the phase is not a physical variable, i.e., it cannot be directly measured but needs to be extracted. However, this is what makes the Kuramoto model general: in fact, it can be obtained via the phase reduction of coupled limit cycle oscillators^{7,106–109}, making it a good approximation of many oscillatory systems.

Finally, the last term denotes the feedback pinning control, where p_i is defined as

$$p_i = \frac{1}{2} K_1^2 \frac{M^2}{\langle k^{(1)} \rangle^2} R_M \tilde{R}_{M,i} \cos(\Psi_M - \tilde{\Psi}_{M,i}), \quad (3)$$

where $M = \sum_{i=1}^N \delta_i$ is the number of controlled nodes, and where we defined the order parameter (2) restricted to the M

controlled nodes,

$$R_M e^{i\Psi_M} = \frac{1}{M} \sum_{j=1}^N \delta_j e^{i\theta_j}, \quad (4)$$

and a slight variation normalized by frequency differences

$$\tilde{R}_{M,i} e^{i\Psi_{M,i}} = \frac{1}{M} \sum_{j=1}^N \delta_j \frac{e^{i\theta_j}}{\omega_j - \omega_i}. \quad (5)$$

The control term (3) is a slightly modified version of the minimally invasive term proposed by Asllani *et al.*³⁵ so that it works on the same principle but is rendered a bit easier to use in practical cases (see Section A for details). Model (1) thus describes the interplay between two antagonistic forces: interactions tend to stabilize full synchronization (at least locally), provided that K_1 and K_2 are large enough, but the pinning control term tends to destabilize it.

Because we use the minimally invasive pairwise Hamiltonian control, we overcome a first issue related to the computational cost required to obtain a many-body control term as in Ref. [100]. On the other hand, as we do not take into account higher-order terms in the control, the latter is not guaranteed to be efficient if K_2 is large in comparison with K_1 ¹⁰⁰. In the following, we will benchmark our working assumption and determine in which cases the minimally invasive pairwise method proves to be sufficient to remove enough synchronization.

To measure the efficiency of the control, we use the time averaged order parameter

$$\hat{R} := \langle R(t) \rangle_{t \in [t_i, t_f]}, \quad (6)$$

where the average has been computed by evaluating $R(t)$ in the interval $[t_i, t_f]$, with t_i large enough to remove the initial transient dynamics. The lower the value of \hat{R} , the better will be the control at reducing the synchronization, hence to result more efficient.

In addition, one can be interested in measuring frequency synchronization, i.e., phase locking. Indeed, in cluster states or twisted states, the phases are desynchronized, $R(t) \approx 0$, but the effective frequencies are (almost) equal. To distinguish these states from complete incoherence, we use the following frequency order parameter¹¹⁰

$$R_\theta(t) = \max \left(1 - \sqrt{\frac{\text{Var}(\dot{\theta}(t))}{\text{Var}(\omega)}}, 0 \right), \quad (7)$$

that lies in $[0, 1]$. This quantity compares the variance of the effective frequencies to that of the natural frequencies. Similarly to the Kuramoto order parameter Eq. (2), $R_\theta(t)$ tends to 1 if the frequencies are synchronized—i.e., the effective frequencies are much less spread than the natural frequencies ω —but tends to 0 if they are not—i.e., they are at least as spread as ω . Similarly to phase synchronization, we report the averaged frequency order parameter

$$\hat{R}_\theta := \langle R_\theta(t) \rangle_{t \in [t_i, t_f]}. \quad (8)$$

As we will see below, the two order parameters will be complementary because the control can achieve full incoherence, $R(t) \approx 0$ and $\hat{R}_\theta \approx 0$, but it can also desynchronize the phases without desynchronizing the frequencies, $R(t) \approx 0$ but $\hat{R}_\theta > 0$. This is because the control term p_i vanishes as $R(t) \approx 0$.

III. THE CASE OF SYNCHRONIZED INITIAL CONDITIONS

We now examine how the presence of higher-order interactions affects the efficiency of the control. To do this, we measure how \hat{R} and \hat{R}_θ change as we vary the triadic coupling strength K_2 and control strength μ . For each value of K_2 and μ , we initialize the system by starting from perfectly synchronized phases $\theta_p = (0, \dots, 0)^T$, with $R(0) = 1$, and let the uncontrolled system, $\mu = 0$, to converge to the fully synchronized state θ_{fs} after a transient time, with $R < 1$ because frequencies are not identical each other. Then, we activate the control, $\mu > 0$, and let the system to converge to its stationary state. Finally, we measure \hat{R} and \hat{R}_θ for that final state, and use them as proxy of control efficiency. In the following, we vary K_2 from 0 to 20 and μ from 0 to 0.25. For simplicity, we start by controlling all nodes, $\delta_i = 1$ for all $i = 1, \dots, N$. The other parameters are set to $N = 100$, $K_1 = 1$ and $\sigma = 0.1$. The chosen hypergraphs topologies are the ones of the hyperrings (see Section III A) and random Erdős-Rényi hypergraphs (see Section III B).

We observe here-after that the larger K_2 , the larger the required μ value that guarantees desynchronization. This means that, when starting from the fully synchronized state, at the center of its attraction basin⁹¹, the increasing of the local stability is the dominant effect and it induces the loss of control's efficiency. In all cases, however, the pairwise minimally invasive control can desynchronize the system if μ is large enough.

A. Hyperrings

First, we focus on hyperring structures. Given N nodes and a range r , a pairwise edge is drawn between node i and each of its $2r$ nearest neighbors on the ring (r on each side). A 2-hyperege is also drawn between node i and any two distinct nodes among these same neighbors. On this structure, system (1) can be written

$$\begin{aligned} \dot{\theta}_i = \omega_i + \frac{K_1}{2r} \sum_{j=i-r}^{i+r} \sin(\theta_j - \theta_i) \\ + \frac{K_2}{2r(r-1)} \sum_{j=i-r}^{i+r} \sum_{k=i-r}^{i+r} \sin(\theta_j + \theta_k - 2\theta_i) + \mu \delta_i p_i, \end{aligned} \quad (9)$$

where we used $\langle k^{(1)} \rangle = 2r$ and $\langle k^{(2)} \rangle = 2r(r-1)$, and the control term p_i is still defined by (3) and we set $\delta_i = 1$ for all i .

Due to the rotational invariance of the underlying substrate, the hyperring supports twisted states^{91,111}. In fact, for pure

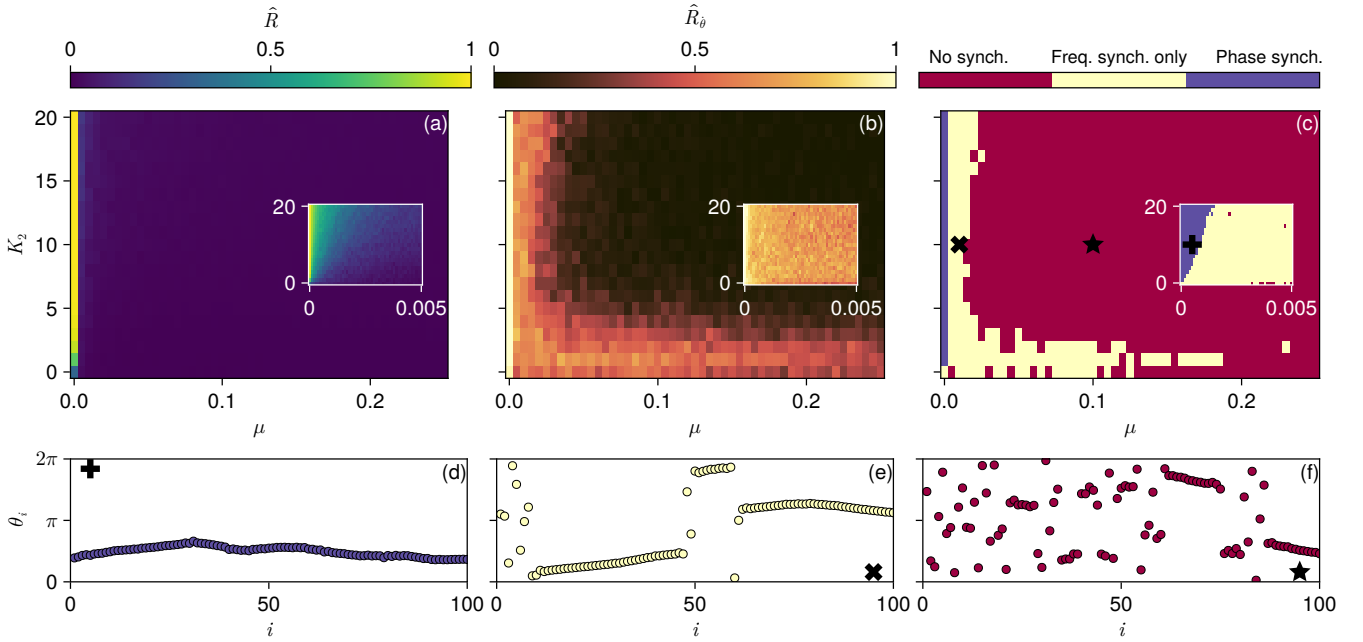


FIG. 1: **Desynchronizing phase oscillators on a hyperring.** We show (a) the level of phase synchronization \hat{R} , and (b) of frequency synchronization \hat{R}_θ as functions of triadic coupling strength K_2 and control strength μ . For each value of (μ, K_2) , we show the value averaged over 50 frequency distributions $\omega \sim \mathcal{N}(0, 0.01)$. Insets zoom in on the low μ region. Panel (c) is obtained by merging the information from panels (a) and (b) and shows the three regimes of the controlled system—phase synchronization (blue, $\hat{R} \geq 0.4$), only frequency synchronization (yellow, $\hat{R} < 0.4$ and $\hat{R}_\theta \geq 0.5$), and no synchronization (red, otherwise)—and associated to the couples (μ, K_2) . Panels (e)–(g) show example snapshots of these regimes as identified with the symbols: plus, cross and star. Parameters are set to $N = 100$, $K_1 = 1$ and $r = 2$.

pairwise interactions $K_2 = 0$, we know that full synchronization and twisted states are the only fixed points of the uncontrolled system $\mu = 0$ ¹¹¹. For the uncontrolled system $\mu = 0$, Ref. [91] also showed that, by increasing $K_2 > 0$, three things occur: the linear stability of twisted states increases, their basin of attraction shrinks, and new disordered states appear and become stable.

We now consider the controlled system, $\mu > 0$. In Fig. 1, we report \hat{R} and \hat{R}_θ as functions of the triadic coupling strength K_2 and the control strength μ , for the case of $r = 2$. We observe that phase synchronization \hat{R} decreases as μ is increased, but increases as K_2 is increased (Fig. 1a). The effect associated to μ is expected—stronger control desynchronizes the system better. The effect of μ and K_2 is similar on frequency synchronization: its increase tends to decrease \hat{R}_θ (Fig. 1b). There is nonetheless a difference: \hat{R}_θ remains high for values of K_2 up to 5.

This phenomenology can be classified into three regimes of increasing disorder, as shown in Fig. 1c. First, for small μ values, i.e., weak control, and regardless of K_2 , the system remains in its initial synchronized regime (blue)—both, phases and frequencies are synchronized—as indicated by large \hat{R} and large \hat{R}_θ . In this phase synchronization regime, phases cluster around a single value and evolve with a common frequency (Fig. 1d). Second, for intermediate values of μ , phases are desynchronized but frequencies are still syn-

chronized (yellow region), as indicated by low \hat{R} but large \hat{R}_θ . This configuration of the two order parameters can represent regimes such as twisted states and cluster states, in which phases are different but oscillators evolve at the same speed. In this frequency synchronization regime, phases appear to cluster around multiple values, but still evolve with a common frequency (Fig. 1e). Notice that, even though this case is close to a cluster state, it is only partially clustered: a proportion of the oscillators display incoherent phases. Generalized order parameters further measure how clustered these states are (see Fig. 7 in Appendix B). Third, for strong control, that is, large μ , no synchronization remains (red region), as indicated by low \hat{R} and low \hat{R}_θ . In this disordered regime, phases evolve at different frequencies and as a result, phases are not coherent (Fig. 1f). In Fig. 1, we classify a given state into the three regimes as follows: if $\hat{R} \geq R_{\text{thr.}}$, then we are dealing with phase synchronization; if $\hat{R} < R_{\text{thr.}}$ but $\hat{R}_\theta \geq 0.5$, then we are dealing with frequency synchronization only; lastly, if both $\hat{R} < R_{\text{thr.}}$ and $\hat{R}_\theta < 0.5$, we consider the system not to be synchronized, neither with respect to phase nor to frequency. We set $R_{\text{thr.}} = 0.4$ based on a preliminary visual inspection of the available data, so that the classification matches actual regimes. The results are qualitatively equivalent in the case $r = 3$ (Fig. 8 Appendix B). Overall, increasing the control strength μ increases desynchronization, as expected.

To further characterize the effect of higher-order interac-

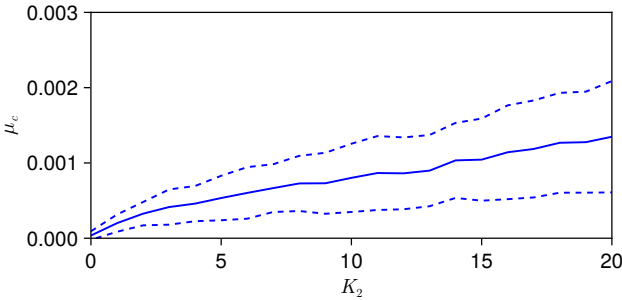


FIG. 2: **Minimum control strength μ_c required to desynchronize $\hat{R} < 0.4$ increases with triadic coupling strength K_2 on hyperring.** We show μ_c averaged (solid line) over 50 frequency distributions ω , and one standard deviation away (dashed lines). Parameters are set to $N = 100$, $K_1 = 1$ and $r = 2$, as in Fig. 1.

tions on control efficiency, we define a critical control strength μ_c as the smallest μ such that $\hat{R} < R_{\text{thr.}}$, that is, such that phases are sufficiently desynchronized. Figure 2 shows that μ_c grows with K_2 , indicating that stronger control is needed to achieve a given level of phase desynchronization as K_2 increases, i.e., as triadic interactions are stronger. Although we know that by increasing K_2 tends to increase the linear stability of synchronization but shrinks its basin size, this monotonic trend suggests that the former effect is dominant over the latter if the initial conditions are synchronized.

Additionally, we observe that the control strength μ necessary to achieve a given level of frequency desynchronization is larger for weaker triadic interactions, $K_2 \leq 5$. This can be seen with \hat{R}_θ (Fig. 1b) and with the yellow region extending to larger μ (Fig. 1c). This behavior may be explained by the fact that, in the uncontrolled system, twisted states are known to have large basins of attraction for small-to-moderate K_2 , which shrinks at larger K_2 ⁹¹. As previously mentioned, note that the minimal control (3), by design, does not directly suppress frequency synchronization. Indeed, the control vanishes if the phases are fully desynchronized, $R = 0$. Therefore, twisted states and clustered states, which are characterized by $R \approx 0$ and $R_\theta \approx 1$, are steady states of the controlled system.

In summary, the pairwise Hamiltonian control considered is able to suppress both phase and frequency synchronization, with phase desynchronization being achieved more readily due to the nature of the control scheme. For synchronized initial conditions, we find that by increasing the higher-order coupling strength K_2 systematically hinders phase desynchronization, as quantified by the monotonic increase of the critical control amplitude μ_c . Frequency synchronization is even more robust for moderate K_2 , owing to hypergraph symmetries and to the fact that it is not directly targeted by the control. Interpreting μ_c as an escape threshold from the synchronized basin, these results indicate that the enhancement of local linear stability induced by higher-order interactions dominates over the simultaneous shrinking of the basin of attraction, thereby making synchronization increasingly resistant to control. While a non-monotonic behavior could, in principle,

arise if basin shrinkage was dominant, however this scenario has not been observed here.

B. Random Hypergraphs

Let us now further validate these results with a more complex topology in system (1). We here consider random hypergraphs obtained from the Erdős-Rényi algorithm⁶⁰. Given a set of N oscillators, we build the hypergraph as follows: we add a 1-hyperedge (edge) for each pair of nodes with probability p_1 and a 2-hyperedge (triangle) between each triplet with probability p_2 . The mean degree and hyperdegree are then $\langle k^{(1)} \rangle = Np_1$ and $\langle k^{(2)} \rangle = N(N-1)p_2$. To compare the results with Section III A, we set $\langle k^{(1)} \rangle = 2r$ and $\langle k^{(2)} \rangle = 2r(r-1)$, with $r = 2$ and 3.

These random hypergraphs do not have rotational invariance, and hence twisted states are no longer supported, except for the synchronized state. In the uncontrolled system, $\mu = 0$, previous research showed that for low K_2 , full synchronization attracts most initial conditions⁹¹. As K_2 is increased, 2-cluster states, and then disordered states, attract most initial conditions instead⁹¹; in parallel, the linear stability of full synchronization also increases even though its attraction basin shrinks.

Results for random hypergraphs are similar to those for hyperrings. Figure 3a shows, for $r = 2$, the phase diagram with the three regimes, obtained by combining the information from \hat{R} and R_θ . It is clear that phase synchronization decreases as μ increases, while it increases as K_2 increases. Stated differently, the heatmap for \hat{R} shows a gradient similar to hyperrings in the (μ, K_2) space (see also Fig. 9a in Appendix B). At lower $K_2 < 5$, the uncontrolled system remains fully synchronized (blue), but the control achieves incoherence (red) for $\mu > 0$. As the triadic coupling strength K_2 is increased, the value of μ required to reach incoherence is larger, and intermediate values desynchronize phases but not the frequencies (yellow). Interestingly, zooming into the region associated to small values of μ (inset) reveals a band of no synchronization (red) at values of μ smaller than the region of frequency synchronization (yellow). The fully synchronized (Fig. 9b) and fully incoherent states (Fig. 9d) are similar to those observed for hyperrings. However, the phase desynchronized ones (Fig. 9c) are different because hyperrings are much more symmetric than random hypergraphs. They can be distinguished from full incoherence because of the spread of their effective frequency distributions (Fig. 9e). Again, we observe that the case $r = 3$ exhibits qualitatively equivalent results (Fig. 10 Appendix B).

Similarly to the case of hyperrings, the minimal control strength μ_c required to reach a given level of phase desynchronization increases with triadic coupling strength K_2 (Fig. 4).

In summary, stronger control is required to desynchronize oscillators—in phase or in frequencies—as higher-order coupling strength is increased, once the system is initialized from fully synchronized initial conditions. Thus, we only observe the influence of the increasing linear stability. These observations are consistent with those from Sec. III A. To be able to

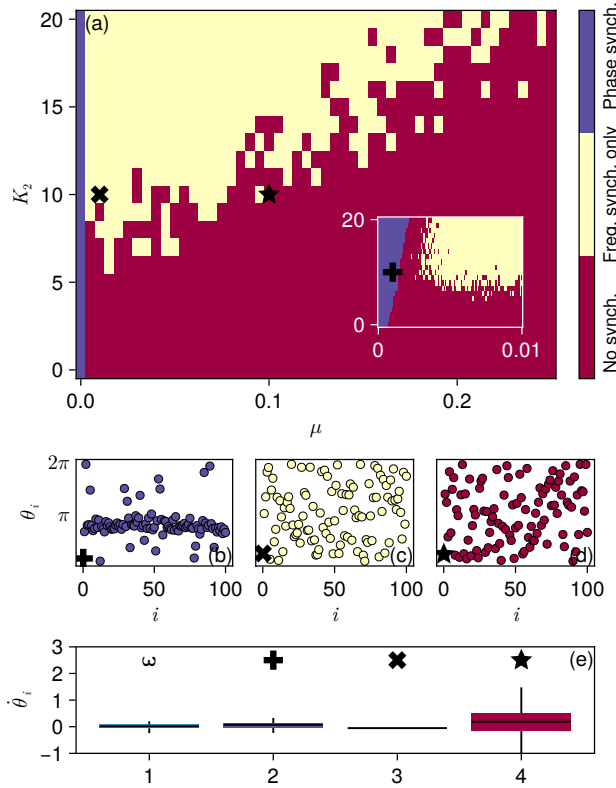


FIG. 3: Desynchronizing phase oscillators on random hypergraphs. We show (a) the division in three zones: phases synchronization ($\hat{R} \geq 0.4$, blue), frequency synchronization only ($\hat{R} < 0.4$ and $\hat{R}_\theta \geq 0.5$, yellow), and no synchronization (otherwise, red). The inset displays details of the low μ region. Panels (b)-(d) show example snapshots of these regimes with $\mu = 0.001$, $\mu = 0.01$ and $\mu = 0.1$, respectively; (e) shows the boxplots of the associated effective frequency distributions, and that of the natural frequencies (left). Parameters are set to $N = 100$, $K_1 = 1$, $\langle k^{(1)} \rangle = 2r$, $\langle k^{(2)} \rangle = 2r(r-1)$ and $r = 2$.

observe the effect of the shrinking of the basin of attraction, we have to move the initial condition away from the fully synchronized state.

IV. THE CASE OF PERTURBED SYNCHRONIZATION AS INITIAL CONDITIONS

In Section III, we observed how the control affects the synchronized state once the system is initialized close to the latter. However, initial conditions can, in general, be arbitrary and not directly related to the synchronous solution. As the control can be seen as a force that tries to push the trajectories out of the basin of attraction of the synchronous state, the actual position of the initial condition plays a crucial role. It is easier for the system to avoid synchronization if the initial conditions are close to the border of the basin, whereas it should be more

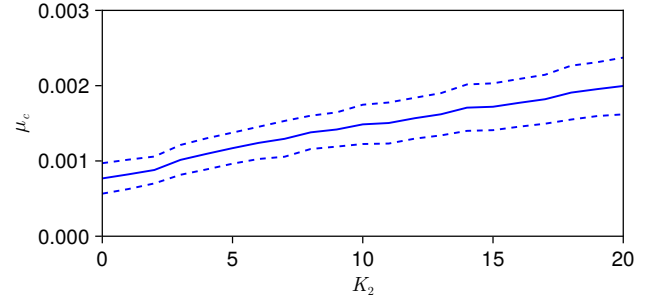


FIG. 4: Minimum control strength μ_c required to desynchronize $\hat{R} < 0.4$ increases with triadic coupling strength K_2 on random hypergraphs. We show μ_c averaged (solid line) over 50 frequency distributions ω , and one standard deviation away (dashed lines). Parameters are, as in Fig. 3, set to $N = 100$, $K_1 = 1$, $\langle k^{(1)} \rangle = 2r$, $\langle k^{(2)} \rangle = 2r(r-1)$ and $r = 2$.

difficult if one starts close to its center. In this respect, it is important to examine how the system behaves by varying the initial conditions. Additionally, we want to compare control schemes where the number of pinned nodes, $M < N$, is varied, which may be easier and less costly to apply in practice.

We consider system (1) and investigate how the level of phase synchronization \hat{R} varies with K_2 , M and the distance between the initial conditions and the phase synchronized state of the system. We modulate this distance with a parameter $\varepsilon \geq 0$ as follows. First, we let the system converge to the phase-synchronized state θ_{fs} as in Section III. Second, we perturb it as

$$\theta_0 = \theta_{fs} + \varepsilon u, \quad (10)$$

where $u \sim U[-\frac{1}{2}, \frac{1}{2}]^N$. Parameter ε controls the initial expected distance from full synchronization. If it is small, the initial conditions tend to lie close to the center of the basin. Note, however, that the basin does not necessarily need to be ball-shaped¹¹². We fix $\mu = 1$, and the intensity of the control is now solely controlled by the number of pinned nodes, M .

As in Section III, numerical examples are shown for $N = 100$, $K_1 = 1$, and for both hyperring and Random Erdős-Renyi structures parametrized by $r = 2$ or 3. Parameter K_2 is varied between 0 to 20 and ε between 0 and 2π . For each value of (K_2, ε) , we performed 50 random realizations of (1) where u is sampled as shown above and the M pinned nodes are distributed uniformly at random among the hypergraph nodes.

A. Hyperrings

Let us first consider the same hyperring structure as in (9). In Fig. 5, we report the results we obtained for \hat{R} , where we fixed $N = 100$, $r = 2$, and $K_1 = 1$ and made ε and K_2 vary. Further results for $r = 3$ are shown in Fig. 11 in Section B, which appear to be qualitatively equivalent.

First, for $M = 0$ (Fig. 5(a)), i.e., the uncontrolled system, and $\varepsilon = 0$, i.e., θ_0 is the "center" of the basin, we observe

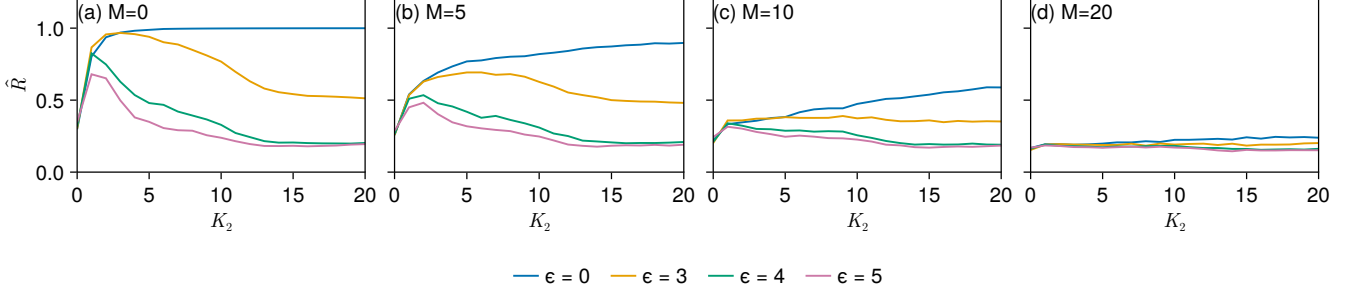


FIG. 5: **Desynchronizing phase oscillators on a hyperring, with partial control.** We show the level of phase synchronization \hat{R} against triadic coupling strength K_2 , by controlling (a)-(d) $M = 0, 5, 10$, and 20 nodes, respectively. For each value of M , we show three values of initial distance to basin center $\epsilon = 0, 3$, and 5 . Other parameters are set to $N = 100$, $r = 2$ and $K_1 = 1$. Order parameter \hat{R} is averaged over 10 random realizations of frequencies ω and 50 of initial conditions θ_0 .

that increasing K_2 leads to an increase in \hat{R} . This aligns with the results shown in Ref. [91], thus indicating deeper synchronization basins.

By increasing ϵ , a non-monotonic behavior emerges as \hat{R} initially increases with K_2 and then decreases. This again aligns with previous work¹⁰², showing that moderate higher-order interactions enhance synchronization, while strong ones hinder synchronization by reducing the basin of attraction. Indeed, as ϵ grows, θ_0 is more likely to lie out of it and then the system goes disordered.

When control is applied with M taking intermediate values, e.g., 5 or 10, (Fig. 5(b)-(c)) and $\epsilon = 0$, then \hat{R} monotonically increases with K_2 . In this regime, the control effectively reduces synchronization, although the presence of higher-order interactions acts as an obstacle. This is the analogous result of Section III A, that is higher-order interactions hinder the control when the system starts near the fully synchronized state.

For the choices $\epsilon = 3, 4$, or 5 , we recover the same type of non-monotonic behavior as above, although the overall \hat{R} values are lower due to the action of the control. Beyond a certain threshold, \hat{R} begins to decrease with increasing K_2 , and the curves tend to coincide with the uncontrolled case.

For $M = 20$ and whatever ϵ value, the \hat{R} curves become nearly constant. Hence, the number of controllers is sufficient to achieve full desynchronization regardless of the value of K_2 . In other words, even when only a fraction of the nodes are pinned, the minimally-invasive Hamiltonian control can desynchronize a higher-order Kuramoto system.

It is also worth commenting on the apparent magnitude of ϵ which might seem large at first glance as the role of ϵ is to implement a relatively small deviation from the initial condition. However, the deviation defined as ϵu means that the initial condition is drawn from a hypercube centered on the fully synchronized state θ_{fs} . The relative volume of this cube is actually $(\frac{\epsilon}{2\pi})^N$, which is of the order of 10^{-10} when $\epsilon = 5$. Thus, the perturbation remains small compared with the size of the full state space.

From these results, we can draw the following conclusions. First, when the system is initialized deep within the basin of attraction and K_2 is not too large, by increasing K_2 in-

creases the strength of the control required for desynchronization. This observation is consistent with the findings reported in^{91,100,113}. Second, when the system is initialized far from full synchrony and K_2 is large, the uncontrolled system does not synchronize, and control primarily serves to accelerate desynchronization and achieve lower \hat{R} values.

B. Random hypergraphs

Let us return to consider Random Erdős-Rényi hypergraphs, as in Section III B. The results we obtain, shown in Fig. 6, are qualitatively similar to the case of hyperrings in Section IV A.

Without control, $M = 0$, and with small values of ϵ (0 and 3), the system remains synchronized regardless of the values of K_2 (Fig. 6(a)). With larger ϵ , the non-monotonic effect appears as \hat{R} slightly increases and then decreases. The non-monotonic nature of the curves is less obvious than in Section IV A because \hat{R} is already close to 1 for $K_2 = 0$.

With control, $M = 10, 20$, and 40 nodes, the overall value of \hat{R} decreases and all curves are pulled downward (Fig. 6(b)-(c)). The non-monotonic behavior of the curve is also preserved, and is even more pronounced, as it is already present at the lowest ϵ values for $M = 20$ and 40 .

These results are the direct consequences of the shrinking of the basin^{91,102}. With moderate K_2 values, the synchronization is strengthened, but with K_2 large the control achieves the desynchronization more easily. This occurs because the control can push more easily the trajectories out of the basin, which has shrunk due to the strong higher-order coupling.

V. CONCLUSION

In this work, we implemented the desynchronizing pairwise minimally invasive Hamiltonian control³⁵ on the higher-order Kuramoto model with pairwise and three-bodies interactions. We modified the control method so that it only requires knowledge of the parameters and states of the controlled nodes with-

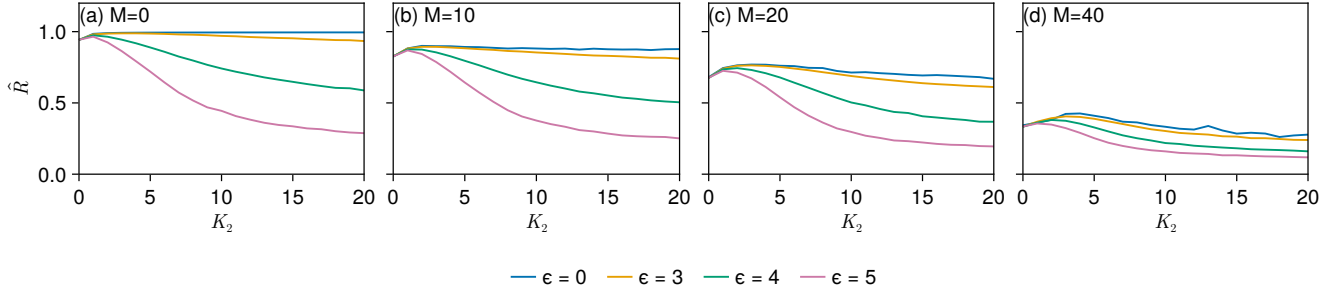


FIG. 6: **Desynchronizing phase oscillators on a random hypergraph, with partial control.** We show the level of phase synchronization \hat{R} against triadic coupling strength K_2 , by controlling (a)-(c) $M = 0, 20$, and 40 nodes, respectively. For each value of M , we show values of initial distance to basin center ϵ between 0 and 2π . Other parameters are set to $N = 100$, $K_1 = 1$, $p_1 = 4/N$ and $p_2 = 4/N^2$. Order parameter \hat{R} is averaged over 10 random realizations of frequencies ω and 50 of initial conditions θ_0 .

out having to know their connectivity. We used hypergraphs with hyperrings structures and then further validated our results on random Erdős-Rényi hypergraphs. We measured the synchronization of the controlled system under several parameterizations to determine whether the higher-order interactions, quantified by the higher-order coupling strength, make the control more effective or not. In other words, we examined where and how the two antagonistic effects of higher-order interactions, i.e., the increasing of linear stability and narrowing of the basin of attraction of synchronization, influence the control efficiency.

We showed that the control was able to desynchronize the system, provided that either a sufficiently large number of nodes is controlled or the control strength is sufficiently large. This is consistent with Ref. [100], where the pairwise version of the control considered in that study was sufficient, in some cases, to desynchronize the higher-order network of oscillators. At the same time, our results go beyond those of Ref. [100] in two respects. First, we consider a minimally invasive version of the control, which improves the previous computationally heavy control term¹⁰⁰. Second, in our case, the pairwise control achieves desynchronization even when all nodes are controlled, whereas this was only observed when pairwise interactions were dominant¹⁰⁰. This difference can be attributed to the topologies considered: all-to-all networks¹⁰⁰ make synchronization much more robust and, therefore, require a more general control strategy to guarantee desynchronization.

When the system starts with synchronized initial conditions, we observed that, by increasing the higher-order coupling strength, the control strength required to desynchronize the system increases. We observed that the control made the system to move from full synchronization to either frequency synchrony without phase synchrony, e.g., cluster or twisted states, or complete incoherence, with no phase or frequency synchrony. The increase in μ_c with K_2 suggests that the effect of increased linear stability of full synchronization is dominant over the shrinking of the attraction basin when it comes to control desynchronization.

In contrast, for other initial conditions, a non-monotonic behavior is observed. Intermediate values of the higher-order coupling strength make the control less effective, whereas larger coupling strengths enhance its efficiency. This behavior appears to reflect the effect of the progressive shrinking of the basin of attraction of the synchronized state. This non-monotonic behavior is in line with other recent studies¹⁰²⁻¹⁰⁴, where an analogous phenomenology was observed in different contexts.

These results shed light on the importance of the dual effect of higher-order interactions, both on linear and basin stability, when control methods are involved. In particular, the non-monotonic nature of this effect could be used for designing efficient control methods and appropriate interaction topologies.

Future work could investigate, for example, the interplay between this non-trivial effect and other complex and more varied topologies, as well as the influence of the choice of controlled nodes, which are selected uniformly at random in this work. Building on recent results on the controllability of higher-order structures⁹², an interesting direction would be to increase the efficiency of the control by targeting specific nodes. Lastly, more application-oriented framework could directly consider non-reduced oscillatory models, as done, e.g., in Ref. [35] for the Stuart-Landau oscillator¹¹⁴, for which this study on the Kuramoto model paves the way.

Acknowledgments:

R.M. acknowledges JSPS KAKENHI 24KF0211 for financial support. M.L. is a Postdoctoral Researcher of the Fonds de la Recherche Scientifique–FNRS.

Author contributions:

M.M. and R.M. conceptualized the study. M.M. and M.L. developed the methodology. M.M. carried out the theoretical analysis and the simulations, validated the results, curated the visualization, and wrote the manuscript. T.C. and M.L. supervised the project. All authors discussed the results, reviewed, and edited the manuscript.

Conflict of interest:

The authors have no conflicts to disclose.

Data availability:

The data that support the findings of this study are available within the article.

¹A. T. Winfree, *The Geometry of Biological Time* (Springer, New York, 1980).

²A. Pikovsky, M. Rosenblum, and J. Kurths, *Synchronization: A Universal Concept in Nonlinear Sciences* (Cambridge University Press, Cambridge, UK, 2003).

³S. H. Strogatz, *Sync: The Emerging Science of Spontaneous Order* (Penguin UK, 2004).

⁴A. Arenas, A. Díaz-Guilera, J. Kurths, Y. Moreno, and C. Zhou, “Synchronization in complex networks,” *Phys. Rep.* **469**, 93–153 (2008).

⁵S. Boccaletti, A. N. Pisarchik, C. I. Del Genio, and A. Amann, *Synchronization: from Coupled Systems to Complex Networks* (Cambridge University Press, Cambridge, 2018).

⁶Y. Kuramoto, “Self-entrainment of a population of coupled non-linear oscillators,” in *International Symposium on Mathematical Problems in Theoretical Physics*, edited by H. Araki (Springer, Berlin, Heidelberg, 1975) pp. 420–422.

⁷Y. Kuramoto, *Chemical Oscillations, Waves, and Turbulence*, edited by H. Haken, Springer Series in Synergetics, Vol. 19 (Springer Berlin Heidelberg, Berlin, Heidelberg, 1984).

⁸S. Strogatz, “From Kuramoto to Crawford: exploring the onset of synchronization in populations of coupled oscillators,” *Physica D* **143**, 1–20 (2000).

⁹J. A. Acebrón, L. L. Bonilla, C. J. P. Vicente, F. Ritort, and R. Spigler, “The Kuramoto model: A simple paradigm for synchronization phenomena,” *Rev. Mod. Phys.* **77**, 137 (2005).

¹⁰M. Bračič Lotrič and A. Stefanovska, “Synchronization and modulation in the human cardiorespiratory system,” *Physica A: Statistical Mechanics and its Applications* **283**, 451–461 (2000).

¹¹C. H. Totz, S. Olmi, and E. Schöll, “Control of synchronization in two-layer power grids,” *Physical Review E* **102**, 022311 (2020).

¹²P. Dallard, T. Fitzpatrick, A. Flint, A. Low, R. R. Smith, M. Willford, and M. Roche, “London millennium bridge: pedestrian-induced lateral vibration,” *Journal of bridge Engineering* **6**, 412–417 (2001).

¹³E. Livne, “Aircraft active flutter suppression: State of the art and technology maturation needs,” *Journal of Aircraft* **55**, 410–452 (2018).

¹⁴Q. Liu, Y. Xu, and J. Kurths, “Active vibration suppression of a novel airfoil model with fractional order viscoelastic constitutive relationship,” *Journal of Sound and vibration* **432**, 50–64 (2018).

¹⁵Q. Liu, R. Muolo, H. Nakao, and Y. Xu, “Flutter suppression enhancement in coupled nonlinear airfoils with intermittent mixed interactions,” *AIAA Journal* **1**, 1–19 (2025).

¹⁶P. J. Uhlhaas and W. Singer, “Neural synchrony in brain disorders: Relevance for cognitive dysfunctions and pathophysiology,” *Neuron* **52**, 155–168 (2006).

¹⁷V. H. Louzada, N. A. Araújo, J. Andrade Jr, and H. J. Herrmann, “How to suppress undesired synchronization,” *Scientific reports* **2**, 658 (2012).

¹⁸D. Wilson and J. Moehlis, “Optimal chaotic desynchronization for neural populations,” *SIAM Journal on Applied Dynamical Systems* **13**, 276 (2014).

¹⁹M. Kringselbach, N. Jenkinson, S. Owen, and T. Aziz, “Translational principles of deep brain stimulation,” *Nat. Rev. Neurosci.* **8**, 623–635 (2007).

²⁰F. Mormann, K. Lehnertz, P. David, and C. E. Elger, “Mean phase coherence as a measure for phase synchronization and its application to the eeg of epilepsy patients,” *Physica D: Nonlinear Phenomena* **144**, 358–369 (2000).

²¹F. da Silva, W. Blanes, S. Kalitzin, J. Parra, P. Suffczynski, and D. Velis, “Dynamical diseases of brain systems: different routes to epileptic seizures,” *IEEE Transactions on Biomedical Engineering* **50**, 540–548 (2003).

²²R. B. Vinter, *Optimal control*, Vol. 2 (Springer, 2010).

²³B. Monga and J. Moehlis, “Optimal phase control of biological oscillators using augmented phase reduction,” *Biological cybernetics* **113**, 161–178 (2019).

²⁴N. Fujii and H. Nakao, “Optimal control for phase locking of synchronized oscillator populations via dynamical reduction techniques,” *Chaos: An Interdisciplinary Journal of Nonlinear Science* **35** (2025), 10.1063/5.0275374.

²⁵R. Grigoriev, M. Cross, and H. Schuster, “Pinning control of spatiotemporal chaos,” *Physical Review Letters* **79**, 2795 (1997).

²⁶F. Sorrentino, M. di Bernardo, F. Garofalo, and G. Chen, “Controllability of complex networks via pinning,” *Physical Review E* **75**, 046103 (2007).

²⁷X. F. Wang and G. Chen, “Pinning control of scale-free dynamical networks,” *Physica A: Statistical Mechanics and its Applications* **310**, 521–531 (2002).

²⁸W. Yu, G. Chen, and J. Lü, “On pinning synchronization of complex dynamical networks,” *Automatica* **2**, 429–435 (2009).

²⁹G. Chen, “Pinning control of complex dynamical networks,” *IEEE Transactions on Consumer Electronics* **68**, 336–343 (2022).

³⁰L. F. R. Turci, P. De Lellis, E. E. N. Macau, M. Di Bernardo, and M. M. R. Simões, “Adaptive pinning control: A review of the fully decentralized strategy and its extensions,” *The European Physical Journal Special Topics* **223**, 2649–2664 (2014).

³¹H. Liu, X. Xu, J.-A. Lu, G. Chen, and Z. Zeng, “Optimizing Pinning Control of Complex Dynamical Networks Based on Spectral Properties of Grounded Laplacian Matrices,” *IEEE Transactions on Systems, Man, and Cybernetics: Systems* **51**, 786–796 (2021).

³²L. Wang, H. P. Dai, H. Dong, Y. Y. Cao, and Y. X. Sun, “Adaptive synchronization of weighted complex dynamical networks through pinning,” *The European Physical Journal B* **61**, 335–342 (2008).

³³O. Gjata, M. Asllani, L. Barletti, and T. Carletti, “Using Hamiltonian control to desynchronize Kuramoto oscillators,” *Phys. Rev. E* **95**, 022209 (2017).

³⁴L. V. Gambuzza and M. Frasca, “Pinning control of chimera states,” *Physical Review E* **94**, 022306 (2016).

³⁵M. Asllani, P. Expert, and T. Carletti, “A minimally invasive neurostimulation method for controlling abnormal synchronisation in the neuronal activity,” *PLoS Comput Biol* **14**, e1006296 (2018).

³⁶M. Moriamé and T. Carletti, “On the location and the strength of controllers to desynchronize coupled kuramoto oscillators,” *Journal of Physics A: Mathematical and Theoretical* **58**, 145202 (2025).

³⁷R. Muolo, L. V. Gambuzza, H. Nakao, and M. Frasca, “Pinning control of chimera states in systems with higher-order interactions,” *Nonlinear Dynamics* **113**, 28233–28255 (2025).

³⁸D. Witthaut and M. Timme, “Kuramoto dynamics in Hamiltonian systems,” *Phys. Rev. E* **90**, 032917 (2014).

³⁹M. Vittot, “Perturbation theory and control in classical or quantum mechanics by an inversion formula,” *J. Phys. A: Math. Gen.* **37**, 6337–6357 (2004).

⁴⁰G. Ciraolo, C. Chandre, R. Lima, M. Vittot, and M. Pettini, “Control Of Chaos In Hamiltonian Systems,” *Celestial Mech Dyn Astr* **90**, 3–12 (2004).

⁴¹F. Battiston, G. Cencetti, I. Iacopini, V. Latora, M. Lucas, A. Patania, J.-G. Young, and G. Petri, “Networks beyond pairwise interactions: Structure and dynamics,” *Physics Reports Networks beyond Pairwise Interactions: Structure and Dynamics*, **874**, 1–92 (2020).

⁴²F. Battiston, E. Amico, A. Barrat, G. Bianconi, G. Ferraz de Arruda, B. Franceschiello, I. Iacopini, S. Kéfi, V. Latora, Y. Moreno, M. M. Murray, T. P. Peixoto, F. Vaccarino, and G. Petri, “The physics of higher-order interactions in complex systems,” *Nat. Phys.* **17**, 1093–1098 (2021).

⁴³G. Bianconi, *Higher-Order Networks: An introduction to simplicial complexes* (Cambridge University Press, Cambridge, 2021).

⁴⁴S. Majhi, M. Perc, and D. Ghosh, “Dynamics on higher-order networks: A review,” *Journal of the Royal Society Interface* **19**, 20220043 (2022).

⁴⁵C. Bick, E. Gross, H. A. Harrington, and M. T. Schaub, “What are higher-order networks?” *SIAM Rev.* **65**, 686–731 (2023).

⁴⁶S. Boccaletti, P. De Lellis, C. Del Genio, K. Alfaro-Bittner, R. Criado, S. Jalan, and M. Romance, “The structure and dynamics of networks with higher order interactions,” *Phys. Rep.* **1018**, 1–64 (2023).

⁴⁷R. Muolo, L. Giambaglia, H. Nakao, D. Fanelli, and T. Carletti, “Turing patterns on discrete topologies: from networks to higher-order structures,” *Proceedings of the Royal Society A* **480**, 20240235 (2024).

⁴⁸A. Millán, H. Sun, L. Giambaglia, R. Muolo, T. Carletti, J. Torres, F. Radicchi, J. Kurths, and G. Bianconi, “Topology shapes dynamics of higher-order networks,” *Nature Physics* **21**, 353–361 (2025).

⁴⁹A. Krawiecki, “Chaotic synchronization on complex hypergraphs,” *Chaos: An Interdisciplinary Journal of Nonlinear Science* **35** (2025), 10.1063/5.0275374.

Solit. Fractals **65**, 44 (2014).

⁵⁰L. V. Gambuzza, F. Di Patti, L. Gallo, S. Lepri, M. Romance, R. Criado, M. Frasca, V. Latora, and S. Boccaletti, “Stability of synchronization in simplicial complexes,” *Nat. Commun.* **12**, 1255 (2021).

⁵¹L. Gallo, R. Muolo, L. Gambuzza, V. Latora, M. Frasca, and T. Carletti, “Synchronization induced by directed higher-order interactions,” *Comm. Phys.* **5**, 236 (2022).

⁵²M. S. Anwar, G. K. Sar, M. Perc, and D. Ghosh, “Collective dynamics of swarmalators with higher-order interactions,” *Commun Phys* **7**, 1–11 (2024).

⁵³M. Anwar, G. Sar, T. Carletti, and D. Ghosh, “A two-dimensional swarmalator model with higher-order interactions,” *SIAM Journal on Applied Mathematics*, in press (2025).

⁵⁴I. León, R. Muolo, H. Nakao, and K. Taga, “Collective dynamics of higher-order Vicsek model emerging from local conformity interactions,” arXiv preprint arXiv:2512.19318 (2025).

⁵⁵S. Kundu and D. Ghosh, “Higher-order interactions promote chimera states,” *Phys. Rev. E* **105**, L042202 (2022).

⁵⁶R. Muolo, T. Njougou, V. L. Gambuzza, T. Carletti, and M. Frasca, “Phase chimera states on nonlocal hyperrings,” *Phys. Rev. E* **109**, L022201 (2024).

⁵⁷Z. Wang, J. Zhu, and X. Liu, “Network stochastic resonance under higher-order interactions,” *Proceedings of the Royal Society A* (2026).

⁵⁸T. Carletti, D. Fanelli, and S. Nicoletti, “Dynamical systems on hypergraphs,” *J. Phys. Complex* **1** (2020), <https://doi.org/10.1088/2632-072X/aba8e1>.

⁵⁹R. Muolo, L. Gallo, V. Latora, M. Frasca, and T. Carletti, “Turing patterns in systems with high-order interactions,” *Chaos, Solitons & Fractals* **166**, 112912 (2023).

⁶⁰I. Iacopini, G. Petri, A. Barrat, and V. Latora, “Simplicial models of social contagion,” *Nat. Commun.* **10**, 2485 (2019).

⁶¹L. Neuhäuser, A. Mellor, and R. Lambiotte, “Multibody interactions and nonlinear consensus dynamics on networked systems,” *Phys. Rev. E* **101**, 032310 (2020).

⁶²G. F. de Arruda, G. Petri, and Y. Moreno, “Social contagion models on hypergraphs,” *Physical Review Research* **2**, 023032 (2020).

⁶³L. DeVille, “Consensus on simplicial complexes: Results on stability and synchronization,” *Chaos* **31**, 023137 (2021).

⁶⁴U. Alvarez-Rodriguez, F. Battiston, G. F. de Arruda, Y. Moreno, M. Perc, and V. Latora, “Evolutionary dynamics of higher-order interactions in social networks,” *Nature Human Behaviour* **5**, 586–595 (2021).

⁶⁵M. Lucas, I. Iacopini, T. Robiglio, A. Barrat, and G. Petri, “Simplicially driven simple contagion,” *Phys. Rev. Res.* **5**, 013201 (2023).

⁶⁶M. Schaub, A. Benson, P. Horn, G. Lippner, and A. Jadbabaie, “Random walks on simplicial complexes and the normalized Hodge 1-Laplacian,” *SIAM Rev.* **62**, 353–391 (2020).

⁶⁷T. Carletti, F. Battiston, G. Cencetti, and D. Fanelli, “Random walks on hypergraphs,” *Phys. Rev. E* **101**, 022308 (2020).

⁶⁸D. Febbe, D. Fanelli, and T. Carletti, “Random walks across dimensions: Exploring simplicial complexes,” arXiv preprint arXiv:2601.16086 (2026).

⁶⁹F. Battiston, C. Bick, M. Lucas, A. Millán, P. Skardal, and Y. Zhang, “Collective dynamics on higher-order networks,” *Nature Reviews Physics* (2026).

⁷⁰I. León and D. Pazó, “Phase reduction beyond the first order: The case of the mean-field complex Ginzburg-Landau equation,” *Phys. Rev. E* **100**, 012211 (2019).

⁷¹E. Gengel, E. Teichmann, M. Rosenblum, and A. Pikovsky, “High-order phase reduction for coupled oscillators,” *Journal of Physics: Complexity* **2**, 015005 (2020).

⁷²C. Bick, T. Böhle, and C. Kuehn, “Higher-order network interactions through phase reduction for oscillators with phase-dependent amplitude,” *Journal of Nonlinear Science* **34**, 77 (2024).

⁷³E. Mau, O. E. Omel’chenko, and M. Rosenblum, “Phase reduction explains chimera shape: When multibody interaction matters,” *Physical Review E* **110**, L022201 (2024).

⁷⁴N. Fujii, K. Taga, R. Muolo, B. Rink, and H. Nakao, “Emergence of higher-order interactions in systems of coupled kuramoto oscillators with time delay,” arXiv preprint arXiv:2512.16193 (2025).

⁷⁵T. Tanaka and T. Aoyagi, “Multistable Attractors in a Network of Phase Oscillators with Three-Body Interactions,” *Phys. Rev. Lett.* **106**, 224101 (2011).

⁷⁶C. Bick, P. Ashwin, and A. Rodrigues, “Chaos in generically coupled phase oscillator networks with nonpairwise interactions,” *Chaos* **26**, 094814 (2016).

⁷⁷P. S. Skardal and A. Arenas, “Abrupt Desynchronization and Extensive Multistability in Globally Coupled Oscillator Simplexes,” *Phys. Rev. Lett.* **122**, 248301 (2019).

⁷⁸P. Skardal and A. Arenas, “Higher order interactions in complex networks of phase oscillators promote abrupt synchronization switching,” *Comm. Phys.* **3**, 1–6 (2020).

⁷⁹A. P. Millán, J. J. Torres, and G. Bianconi, “Explosive Higher-Order Kuramoto Dynamics on Simplicial Complexes,” *Phys. Rev. Lett.* **124**, 218301 (2020).

⁸⁰M. Lucas, G. Cencetti, and F. Battiston, “Multiorder Laplacian for synchronization in higher-order networks,” *Phys. Rev. Res.* **2**, 033410 (2020).

⁸¹K. Kovalenko, X. Dai, K. Alfar-Bittner, A. M. Raigorodskii, M. Perc, and S. Boccaletti, “Contrarians Synchronize beyond the Limit of Pairwise Interactions,” *Phys. Rev. Lett.* **127**, 258301 (2021).

⁸²S. Adhikari, J. Restrepo, and P. Skardal, “Synchronization of phase oscillators on complex hypergraphs,” *Chaos* **33** (2023).

⁸³Y. Zhang, M. Lucas, and F. Battiston, “Higher-order interactions shape collective dynamics differently in hypergraphs and simplicial complexes,” *Nature communications* **14**, 1605 (2023).

⁸⁴I. León, R. Muolo, S. Hata, and H. Nakao, “Higher-order interactions induce anomalous transitions to synchrony,” *Chaos* **34**, 013105 (2024).

⁸⁵R. Fariello and M. A. de Aguiar, “Third order interactions shift the critical coupling in multidimensional Kuramoto models,” *Chaos, Solitons & Fractals* **187**, 115467 (2024).

⁸⁶G. Costa, M. Novaes, and M. de Aguiar, “Bifurcations in the Kuramoto model with external forcing and higher-order interactions,” *Chaos* **34** (2024).

⁸⁷H. Huh and D. Kim, “Critical threshold for synchronizability of high-dimensional Kuramoto oscillators under higher-order interactions,” *Chaos* **34** (2024).

⁸⁸X. Wang, H. Li, Q. Dai, and J. Yang, “Coexistence of multistable synchronous states in a three-oscillator system with higher-order interaction,” *Phys. Rev. E* **110**, 034311 (2024).

⁸⁹I. León, R. Muolo, S. Hata, and H. Nakao, “Theory of phase reduction from hypergraphs to simplicial complexes: a general route to higher-order Kuramoto models,” *Physica D* (2025), [10.1016/j.physd.2025.134858](https://doi.org/10.1016/j.physd.2025.134858).

⁹⁰N. Namura, R. Muolo, and H. Nakao, “Optimal interaction functions realizing higher-order kuramoto dynamics with arbitrary limit-cycle oscillators,” *Chaos* **36** (2026).

⁹¹Y. Zhang, P. S. Skardal, F. Battiston, G. Petri, and M. Lucas, “Deeper but smaller: Higher-order interactions increase linear stability but shrink basins,” *Sci. Adv.* **10**, eado8049 (2024).

⁹²C. Chen, A. Surana, A. M. Bloch, and I. Rajapakse, “Controllability of hypergraphs,” *IEEE Transactions on Network Science and Engineering* **8**, 1646–1657 (2021).

⁹³P. De Lellis, F. Della Rossa, F. Lo Iudice, and D. Liuzza, “Pinning control of hypergraphs,” *IEEE Control Systems Letters* **7**, 691–696 (2022).

⁹⁴F. Della Rossa, D. Liuzza, F. Lo Iudice, and P. De Lellis, “Emergence and control of synchronization in networks with directed many-body interactions,” *Physical Review Letters* **131**, 207401 (2023).

⁹⁵P. De Lellis, F. Della Rossa, F. Lo Iudice, and D. Liuzza, “Pinning control of linear systems on hypergraphs,” *European Journal of Control* **74**, 100836 (2023).

⁹⁶T. Shi, Y. Qin, Q. Yang, Z. Ma, and K. Li, “Synchronization of directed uniform hypergraphs via adaptive pinning control,” *Physica A: Statistical Mechanics and its Applications* **615**, 128571 (2023).

⁹⁷R. Rizzello and P. De Lellis, “Pinning control in networks of nonidentical systems with many-body interactions,” *IEEE Control Systems Letters* **8**, 1313–1318 (2024).

⁹⁸R. Xia and L. Xiang, “Pinning control of simplicial complexes,” *European Journal of Control* **77**, 100994 (2024).

⁹⁹K. Li, Y. Lin, and J. Wang, “Synchronization of multi-directed hypergraphs via adaptive pinning control,” *Chaos, Solitons & Fractals* **184**, 115000 (2024).

¹⁰⁰M. Moriamé, M. Lucas, and T. Carletti, “Hamiltonian control to desyn-

chronize Kuramoto oscillators with higher-order interactions," *PRE* **111** (2025), [/10.1103/PhysRevE.111.044307](https://doi.org/10.1103/PhysRevE.111.044307).

¹⁰¹Z. Wang, W. Qi, J. Zhu, and X. Liu, "How do higher-order interactions shape the energy landscape?" *Phys. Rev. E* **112**, 064217 (2025).

¹⁰²R. Muolo, H. Nakao, and M. Coraggio, "When higher-order interactions enhance synchronization: the case of the Kuramoto model on random hypergraphs," arXiv preprint arXiv:2508.10992 (2025).

¹⁰³Z. Wang, J. Zhu, and X. Liu, "Moderate higher-order interactions enhance stability while preserving basin structure," arXiv preprint arXiv:2510.13321 (2025).

¹⁰⁴P. Skardal, F. Battiston, M. Lucas, M. Mizuhara, G. Petri, and Y. Zhang, "Mixed higher-order coupling stabilizes new states," arXiv preprint arXiv:2510.09387 (2025).

¹⁰⁵Note that the three-body interaction can take two different forms^{69,89}: $\sin(\theta_j + \theta_k - 2\theta_i)$, i.e., $(1, 1, -2)$ interaction⁹⁰, and $\sin(2\theta_j - \theta_k - \theta_i)$, i.e., $(2, -1, -1)$ interaction⁹⁰. Full synchronization in both higher-order Kuramoto models behaves in a qualitatively analogous way with respect to the variations of the coupling strengths¹⁰². Here, for sake of simplicity, we only consider on the $(1, 1, -2)$ interaction.

¹⁰⁶H. Nakao, "Phase reduction approach to synchronisation of nonlinear oscillators," *Contemp. Phys.* **57**, 188–214 (2016).

¹⁰⁷B. Pietras and A. Daffertshofer, "Network dynamics of coupled oscillators and phase reduction techniques," *Physics Reports* **819**, 1–105 (2019).

¹⁰⁸B. Monga, D. Wilson, T. Matchen, and J. Moehlis, "Phase reduction and phase-based optimal control for biological systems: a tutorial," *Biological cybernetics* **113**, 11–46 (2019).

¹⁰⁹Y. Kuramoto and H. Nakao, "On the concept of dynamical reduction: the case of coupled oscillators," *Phil. Trans. R. Soc. A* **377**, 20190041 (2019).

¹¹⁰J. Newman, J. Rowland Adams, P. T. Clemson, and A. Stefanovska, "An order parameter for synchronisation of angular velocities," *The European Physical Journal Special Topics* , 1–13 (2025).

¹¹¹D. A. Wiley, S. H. Strogatz, and M. Girvan, "The size of the sync basin," *Chaos: An Interdisciplinary Journal of Nonlinear Science* **16** (2006), [10.1063/1.2165594](https://doi.org/10.1063/1.2165594).

¹¹²Y. Zhang and S. H. Strogatz, "Basins with tentacles," *Phys. Rev. Lett.* **127**, 194101 (2021).

¹¹³S. von der Gracht, E. Nijholt, and B. Rink, "Higher-order interactions lead to 'reluctant' synchrony breaking," *Proceedings of the Royal Society A* **480**, 20230945 (2024).

¹¹⁴H. Nakao, "Complex ginzburg-landau equation on networks and its non-uniform dynamics," *The European Physical Journal Special Topics* **223**, 2411–2421 (2014).

¹¹⁵C. C. Gong and A. Pikovsky, "Low-dimensional dynamics for higher-order harmonic, globally coupled phase-oscillator ensembles," *Phys. Rev. E* **100**, 062210 (2019).

Appendix A: Computation of the control term

The original pairwise Hamiltonian pinning control was developed in Ref. [33], based on Hamiltonian control theory^{39,40} and the Hamiltonian embedding of the Kuramoto model³⁸. This method has then been perfected in two ways.

In Ref. [35], the authors went a step further by reducing the control term's magnitude in order to make the method minimally invasive. In short, they isolated the dominant terms so that the control adapts its magnitude to grow with K_1^2 and $R(t)$. It is thus significant only when the system is (likely to be) synchronized, i.e., when K_1 and/or R are large, but negligible otherwise. By doing so, the authors made the control method more likely to be implemented in a practical case, e.g., to prevent the emergence of seizures.

On the other hand, it was shown¹⁰⁰ that the (not minimally invasive) pairwise control can (partially) desynchronize the higher order system in several cases, namely if the pairwise interactions are strong and the higher order ones weak. In the opposite case, Ref. [100] proposes to use the higher-order generalization of the Hamiltonian control which can desynchronize the higher-order system in any case. However, it comes with the cost of an increasing number of high magnitude terms, which would make it even harder to implement in a practical context.

In this work, we propose to use the minimally invasive version of the pairwise control in order to desynchronize higher-order systems of Kuramoto oscillators. By doing so, we accept that in some cases the control will not achieve its goal, but, on the other hand, we can understand more precisely the cases where this minimal control action is sufficient and when it should be reinforced with higher-order terms.

We nevertheless introduce some slight modifications from the method used in Ref. [35]. (i) Whereas the latter requires the knowledge of the pairwise topology of the system, which is a real constraint in a practical context, we relax this by computing the control term as if the pinned nodes were connected by a clique. It makes the control both easier to compute and potentially more powerful (see below). (ii) We restrict the computation of the control term to the very M pinned nodes. The control acts thus as a proper feedback loop: from the measure of the phases and natural frequencies of the pinned nodes only, the control term is computed and then injected into those nodes' dynamics without requiring the knowledge of the global order parameter like in Ref. [35].

Let us now develop how the control term p_i of Eq. (1) is defined, by following the same methods of Refs [33 and 35] but taking into account the little modifications (i) and (ii) we have just mentioned. The idea of Ref. [33] consists in adding, to a subset of M nodes, an additive term

$$h_i = \begin{cases} -\frac{1}{2} \frac{\partial \{\Gamma V, V\}}{\partial I_i} \Big|_{T_{1/2}} & \text{if } i = 1, \dots, M, \\ 0 & \text{otherwise,} \end{cases} \quad (\text{A1})$$

where

$$H(\mathbf{I}, \boldsymbol{\theta}) = H_0(\mathbf{I}) + V(\mathbf{I}, \boldsymbol{\theta}) = \sum_i I_i \omega_i + \frac{K}{\langle k^{(1)} \rangle} \sum_{ij} A_{ij} \sqrt{I_i I_j} (I_j - I_i) \sin(\theta_j - \theta_i) \quad (\text{A2})$$

is a Hamiltonian function of action and angles variables I_i and θ_i . It is such that the resulting Hamiltonian system embeds the classical Kuramoto Model on the invariant torus $T_{1/2} = \{(\mathbf{I}, \boldsymbol{\theta}) \mid \forall i : I_i = 1/2\}$. This function exists in higher-order versions but we here restrict ourselves to the pairwise case. Finally, Γ is the pseudoinverse operator of H_0 .

The term h_i actually uses all the network parameters, i.e., K_1 , N , the entries A_{ij} , the frequencies ω_i and the phases θ_i (such that the mentioned indexes $i, j \in 1, \dots, M$) and is computed (for $i = 1, \dots, M$) as

$$\begin{aligned} h_i = & \frac{1}{2} \left(\frac{K_1}{\langle k^{(1)} \rangle} \sum_{k=1}^M A_{ki} \cos(\theta_k - \theta_i) \right) \times \left(-\frac{K_1}{\langle k^{(1)} \rangle} \sum_{k=1}^M A_{ki} \frac{\cos(\theta_k - \theta_i)}{\omega_k - \omega_i} \right) \\ & - \frac{1}{2} \left(-\frac{K_1}{\langle k^{(1)} \rangle} \sum_{k=1}^M A_{ki} \sin(\theta_k - \theta_i) \right) \times \left(-\frac{K_1}{\langle k^{(1)} \rangle} \sum_{k=1}^M A_{ki} \frac{\sin(\theta_k - \theta_i)}{\omega_k - \omega_i} \right) \\ & + \frac{1}{2} \sum_{j=1}^M \left\{ \left(-\frac{K_1}{\langle k^{(1)} \rangle} A_{ij} \cos(\theta_j - \theta_i) \right) \times \left(-\frac{K_1}{\langle k^{(1)} \rangle} \sum_{k=1}^M A_{kj} \frac{\cos(\theta_k - \theta_j)}{\omega_k - \omega_j} \right) \right. \\ & \left. - \left(-\frac{K_1}{\langle k^{(1)} \rangle} \sum_{k=1}^M A_{jk} \sin(\theta_k - \theta_j) \right) \times \left(\frac{K_1}{\langle k^{(1)} \rangle} A_{ij} \frac{\sin(\theta_j - \theta_i)}{\omega_j - \omega_i} \right) \right\}. \end{aligned} \quad (\text{A3})$$

As said above (i), we here propose compute the pinning control term in the same way that if \mathbf{A} actually defined a M -clique

connecting the M pinned nodes all together, in other words

$$\begin{aligned}\hat{h}_i &:= \frac{1}{2} \left(\frac{K_1}{\langle k^{(1)} \rangle} \sum_{k=1}^M \cos(\theta_k - \theta_i) \right) \times \left(-\frac{K_1}{\langle k^{(1)} \rangle} \sum_{k=1}^M \frac{\cos(\theta_k - \theta_i)}{\omega_k - \omega_i} \right) \\ &\quad - \frac{1}{2} \left(-\frac{K_1}{\langle k^{(1)} \rangle} \sum_{k=1}^M \sin(\theta_k - \theta_i) \right) \times \left(-\frac{K_1}{\langle k^{(1)} \rangle} \sum_{k=1}^M \frac{\sin(\theta_k - \theta_i)}{\omega_k - \omega_i} \right) \\ &\quad + \frac{1}{2} \sum_{j=1}^M \left\{ \left(-\frac{K_1}{\langle k^{(1)} \rangle} \cos(\theta_j - \theta_i) \right) \times \left(-\frac{K_1}{\langle k^{(1)} \rangle} \sum_{k=1}^M \frac{\cos(\theta_k - \theta_j)}{\omega_k - \omega_j} \right) \right. \\ &\quad \left. - \left(-\frac{K_1}{\langle k^{(1)} \rangle} \sum_{k=1}^M \sin(\theta_k - \theta_j) \right) \times \left(\frac{K_1}{\langle k^{(1)} \rangle} \frac{\sin(\theta_j - \theta_i)}{\omega_j - \omega_i} \right) \right\}.\end{aligned}\tag{A4}$$

This approach has the double advantage of freeing us from the need to know the actual connections A_{ij} between the pinned nodes and of using the control at the maximum of its potential power, as all the possible terms are considered in the sums (no $A_{ij} = 0$ as is (A3)).

Then, we can write³⁵

$$\hat{h}_i = \frac{1}{2} K_1^2 \frac{M^2}{\langle k^{(1)} \rangle^2} R_M \hat{R}_{M,i} \cos(\Psi_M - \hat{\Psi}_{M,i}) + \mathcal{B}_i, \tag{A5}$$

where \mathcal{B}_i is a term that, in general, can be neglected³⁵. The latter can thus be removed without losing the control efficiency. The final resulting pinning control term, that is minimally invasive³⁵, is the term (3). Note that here, R_M is used in (A5) instead of R like in Ref. [35], so that the control term computation do not require the knowledge of any feature of the uncontrolled nodes (ii).

Appendix B: Supplementary figures

This Section displays the Supplementary Figures which complement the numerical results of Sections III and IV. Its structure is set in parallel with those Sections.

1. The case of synchronized initial conditions

Let us first introduce the notion of n^{th} order parameter¹¹⁵

$$R_{(n)} e^{i\Psi_{(n)}} = \frac{1}{N} \sum_{j=1}^N e^{i\mu\theta_j}, \tag{B1}$$

which are used to detect cases of clustered synchronization. Namely, $R_{(n)} \in [0, 1]$ and

$$R_{(n)}(t) = 1 \iff \forall i = 1, \dots, N : \theta_i \in \left\{ \theta_1(t) + \frac{2\pi j}{n} \mid j = 1, \dots, n \right\}.$$

In other words, $R_{(n)} = 1$ when the phases are distributed into n groups of equally-valued members that are separated by an angle of $\frac{2\pi}{n}$. If the phases are not perfectly n -clustered, i.e., the members of a cluster have close phases but not exactly equal and/or the distance between the clusters are not exactly $\frac{2\pi}{n}$, then $0 \ll R_{(n)} < 1$. Note however that the groups do not necessarily have the same size. In the same way as in (6), we define

$$\hat{R}_{(n)} := \langle R_{(n)}(t) \rangle_{t \in [t_i, t_f]} \tag{B2}$$

to measure the presence of cluster synchronization.

Respectively in Fig. 7(a) and Fig. 7(b) we report the values of $\hat{R}_{(2)}$ and $\hat{R}_{(3)}$ obtained from the same trajectories that in Fig. 1. We can first remark that for $\mu = 0$ the values of $\hat{R}_{(2)}$ and $\hat{R}_{(3)}$ are very close to \hat{R} observed in Fig. 1(a), i.e., they rapidly grow with K_2 and are very close to 1 if $K_2 \geq 3$. This is expected, as a straightforward computation can show that $R_{(1)} = 1 \Rightarrow R_{(2)} = 1$ and $R_{(1)} = 1 \Rightarrow R_{(2)} = 1$, although the contrapositive is not true. With $\mu > 0$, i.e., control activated, $\hat{R}_{(2)}$ and $\hat{R}_{(3)}$ are in general

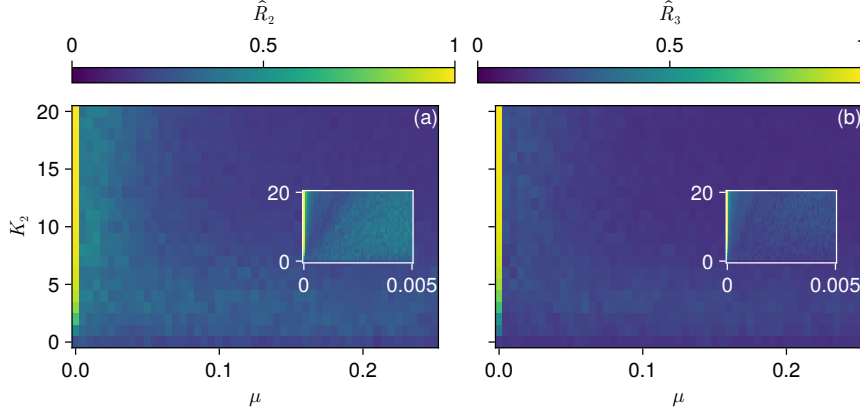


FIG. 7: **Extention of Fig. 1** encoding \hat{R}_2 (panel (a)) and \hat{R}_3 (panel (b)), the order parameters detecting resp. 2- and 3-cluster synchronization, as function of K_2 and μ . We use a hyperring structure with $r = 2$. As in Fig. 1, each point (K_2, μ) is the value averaged over 50 frequency distributions $\omega \sim \mathcal{N}(0, \sigma^2)$, $N = 100$, $K_1 = 1$, $\omega \sim \mathcal{N}(0, \sigma^2)$ and $\sigma = 0.1$.

quite low, meaning that there are no notable presence of clustered synchronization. However, one can notice that $\hat{R}_{(2)}$ reaches intermediate values around 0.5 in a region that corresponds to the "frequency synchronization only" zone in Fig. 1(b-c). This is in line with the partially-clustered trajectory that we observe in Fig. 1(e), that looks like a 3-cluster at first glance but is actually closer to a 2-cluster because of the angular nature of the data (the two first groups we see on the figure actually form one single group, as their members are located close to 0 and 2π , respectively).

Fig. 8 shows the results of the same experiment on hyperrings with $r = 3$ and is analogous to Fig. 1 (case $r = 2$). We can observe qualitatively equivalent results as in the case $r = 2$, as the $\hat{R} \geq R_{\text{thr.}}$ and $\hat{R}_\theta \geq 0.5$ have the same shape. The main difference is that those zones, i.e., the phase synchrony and frequency synchrony zones, are wider than in the $r = 2$ case. Indeed, with $r = 3$ the links and triangles are denser in the hypergraph, i.e. there are more interactions between the nodes, which causes an increased stability of the synchronized state. The control goal is therefore harder to achieve.

In Fig. 9 we show supplementary panels related to Fig. 3. Panels (a-b) exhibit resp. the \hat{R} and \hat{R}_θ data that correspond to the aggregated panel Fig. 3(a). We observe no presence of cluster synchronization in this case.

Fig. 10 displays the analogous results for random hypergraph structures with $r = 3$. We can observe that the results are in general qualitatively equivalent to the case $r = 2$ in Fig. 3. The two main differences are that the phase synchrony region is larger

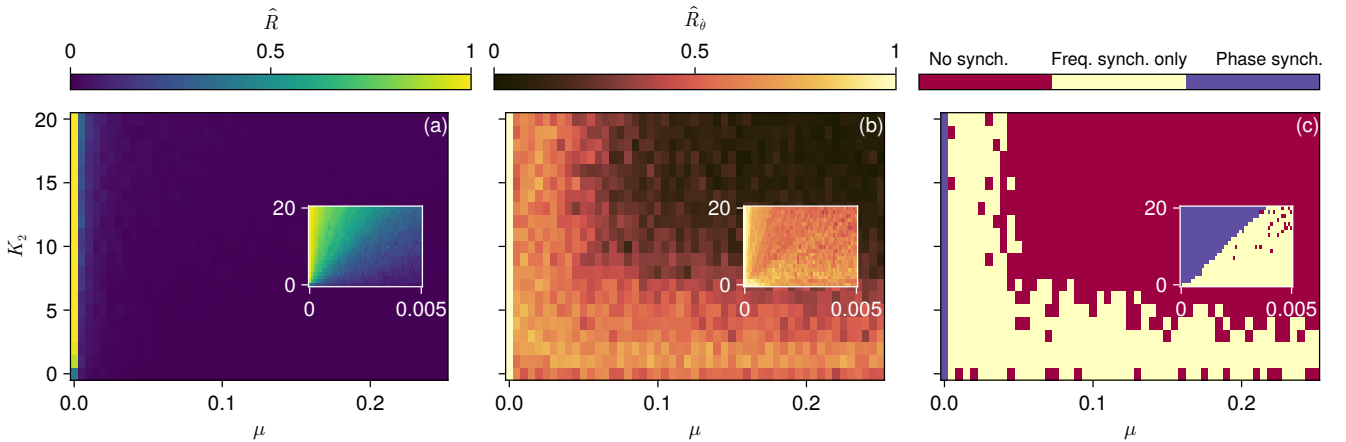


FIG. 8: **Desynchronizing phase oscillators on a hyperring with $r = 3$** . Similarly to Fig. 1, we show (a) the level of phase synchronization \hat{R} , (b) of frequency synchronization \hat{R}_θ and (c) the three regimes of the controlled system—phase synchrony (blue, $\hat{R} \geq 0.4$), only frequency synchronization (yellow, $\hat{R} < 0.4$ and $\hat{R}_\theta \geq 0.5$), and no synchronization (red, otherwise)—, all as function of (K_2, μ) . For each value of (K_2, μ) , we show the value averaged over 50 frequency distributions $\omega \sim \mathcal{N}(0, \sigma^2)$. Parameters are set to $N = 100$, $K_1 = 1$, $\sigma = 0.1$ and $r = 3$.

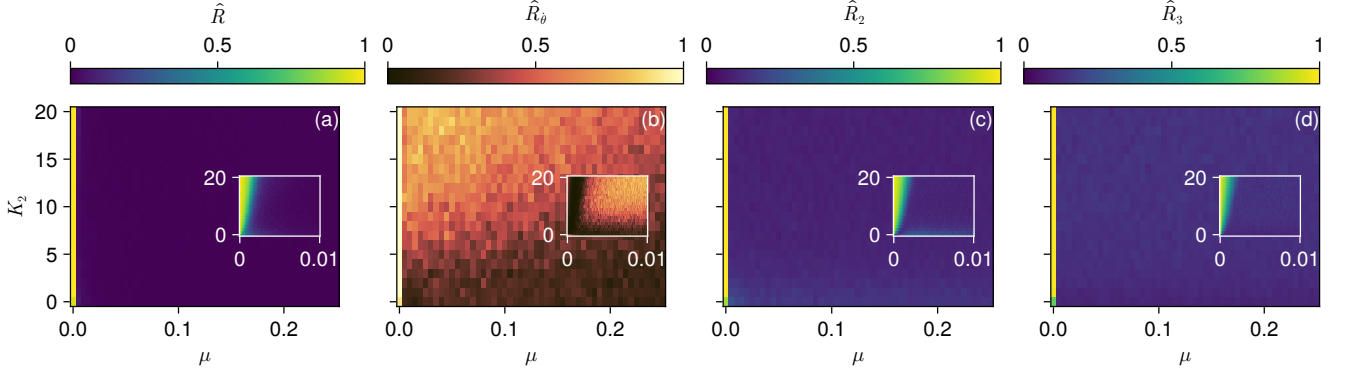


FIG. 9: **Extension of Fig. 3**, displaying (a) \hat{R} , (b) \hat{R}_θ , (c) $\hat{R}_{(2)}$ and (d) $\hat{R}_{(3)}$, all as a function of K_2 and μ . As in Fig. 3, the trajectories are drawn from random hypergraphs with parameters set as $N = 100$, $K_1 = 1$, $\hat{R}_{(2)} = 0.1$, $\langle k^{(1)} \rangle = 2r$, $\langle k^{(2)} \rangle = 2r(r-1)$ and for each value of (K_2, μ) , we show the value averaged over 50 frequency distributions $\omega \sim \mathcal{N}(0, \sigma^2)$.

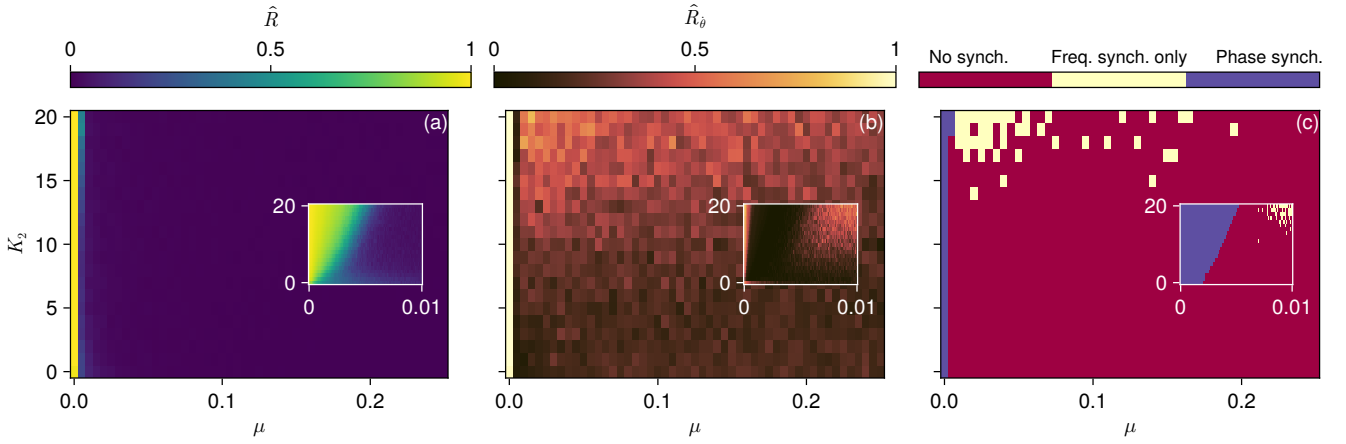


FIG. 10: **Desynchronizing phase oscillators on a Random hypergraphs with $r = 3$** . Similarly to Fig. 3, we show (a) the level of phase synchronization \hat{R} , (b) of frequency synchronization \hat{R}_θ and (c) the three regimes of the controlled system—phase synchronization (blue, $\hat{R} \geq 0.4$), only frequency synchronization (yellow, $\hat{R} < 0.4$ and $\hat{R}_\theta \geq 0.5$), and no synchronization (red, otherwise)—, all as function of K_2 and μ . For each value of (K_2, μ) , we show the value averaged over 50 frequency distributions $\omega \sim \mathcal{N}(0, \sigma^2)$ together with 50 realization of the higher-order Erdős-Renyi algorithm. Parameters are set to $N = 100$, $K_1 = 1$, $\sigma = 0.1$ and $r = 3$.

while the region with only frequency synchronization is narrower. This may be explained by the increasing of both pairwise and higher-order interactions, which increase the local stability of phase synchronization and make the control goal harder to achieve. Moreover, other phase locking states are also harder to attain because of the absence of symmetry in the topology.

2. The case of unsynchronized initial conditions

Figs. 5 and 6 are respectively analogous to Figs. 11 and 12 with $r = 3$. They display qualitatively equivalent plots.

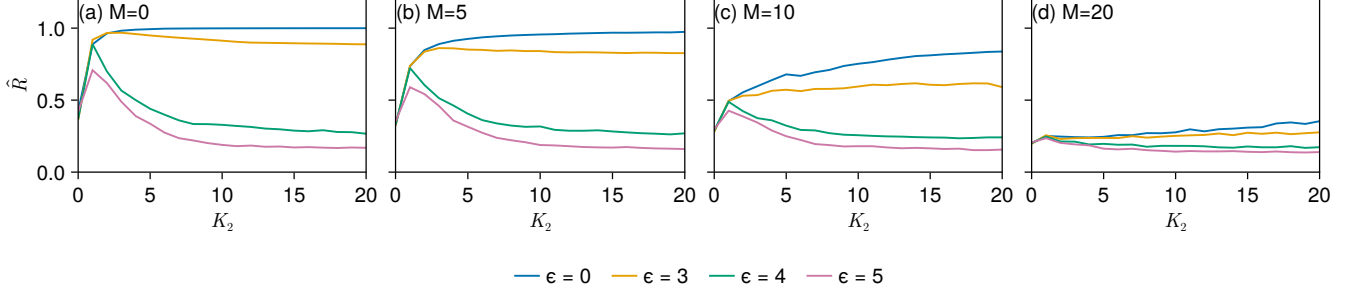


FIG. 11: **Desynchronizing phase oscillators on a hyperring with $r = 3$.** Similarly to Fig. 5: we show \hat{R} as a function of K_2 and ϵ , by controlling (a)-(d) $M = 0, 5, 10$, and 20 nodes, respectively. Other parameters are set to $N = 100$, $r = 2$ and $K_1 = 1$. Order parameter \hat{R} is averaged over 10 random realizations of frequencies ω and 50 of initial conditions θ_0 .

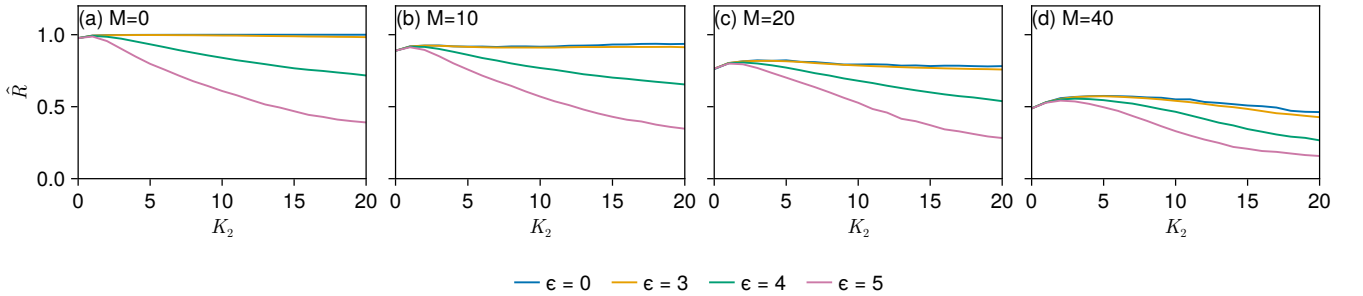


FIG. 12: **Desynchronizing phase oscillators on a hyperring with $r = 3$.** Similarly to Fig. 5: we show \hat{R} as a function of K_2 and ϵ , by controlling (a)-(d) $M = 0, 5, 10$, and 20 nodes, respectively. Other parameters are set to $N = 100$, $r = 2$ and $K_1 = 1$. Order parameter \hat{R} is averaged over 50 random realizations of frequencies ω , each with a hypergraphs generated via the higher-order Erdős-Renyi procedure and 50 of initial conditions θ_0 .